Peer-reviewed version available at Materials 2019, 12, 2232; doi:10.3390/ma12142232

Article

Electrical Properties of Low-Temperature Processed Sn-doped In_2O_3 thin films: The Role of Microstructure and Oxygen Content and the Potential of Defect Modulation Doping

Getnet K. Deyu [1,2], Jonas Hunka [1], Hervé Roussel [2], Joachim Brötz [3], Daniel Bellet [2] and Andreas Klein [1,*]

1 Technische Universität Darmstadt, Department of Materials and Earth Sciences, Electronic Structure of Materials, Otto-Berndt-Straße 3, 64287 Darmstadt, Germany
2 Univ. Grenoble Alpes, CNRS, Grenoble INP, LMGP, 38 000 Grenoble, France
3 Technische Universität Darmstadt, Department of Materials and Earth Sciences, Structural Research, Otto-Berndt-Straße 3, 64287 Darmstadt, Germany
* Correspondence: aklein@esm.tu-darmstadt.de; Tel.: +49-6151-16-20772

Abstract: Low-temperature processed ITO thin films offer the potential of overcoming the doping limit by suppressing the equilibrium of compensating oxygen interstitial defects. To elucidate this potential, electrical properties of Sn-doped In_2O_3 (ITO) thin films are studied in dependence on film thickness. In-operando conductivity and Hall effect measurements during annealing of room temperature deposited films with different film thickness in different environments allow to discriminate between the effects of crystallization, grain growth, donor activation and oxygen diffusion on carrier concentrations and mobilities. At 200 °C, a control of carrier concentration by oxygen incorporation or extraction is only possible for very thin films. The electrical properties of thicker films deposited at room temperature are mostly affected by grain size. The remaining diffusivity of compensating oxygen defects at 200 °C is sufficient to screen the high Fermi level induced by deposition of Al_2O_3 using atomic layer deposition (ALD), which disables the use of defect modulation doping at this temperature. The results indicate that achieving higher carrier concentrations requires a control of the oxygen pressure during deposition in combination with seed layers to enhance crystallinity or the use of near room temperature ALD.

Keywords: ITO; electrical properties; doping limits; modulation doping; thickness dependence; low-temperature deposition

1. Introduction

Transparent conductive oxides (TCOs) are key materials for electrodes in display and solar cell technologies [1–6]. The most prominent examples are Sn-doped In_2O_3 (ITO), Al-doped ZnO (AZO) and F-doped SnO_2 (FTO), which are degenerately doped n-type semiconductors. Highest electrical conductivities of $\sim 10^4$ S/cm are obtained with ITO having carrier concentrations of $1 - 2 \times 10^{21}$ cm^{-3} and mobilities of ~ 40 cm^2/Vs [7]. Even higher conductivities are desirable, for example to reduce optical losses in solar cells by using thinner TCOs or wider cells in thin film modules. The conductivity can be increased either by a higher carrier concentration or a higher carrier mobility.

If thermodynamic equilibrium of defect concentrations can be established, the concentration of free electrons in TCOs is limited by formation of self-compensating intrinsic defects [6,8–10]. In the case of donor-doped In_2O_3, the compensating defect species is interstitial oxygen [10–15]. Consequently, the diffusion of oxygen is required to establish defect equilibrium. At the limit of electrical conductivity, the addition of more donors does then not result in an increase of the concentration of free electrons but in that of interstitial oxygen. The carrier concentration can also be limited if the dopants are not

Peer-reviewed version available at Materials 2019, 12, 2232; doi:10.3390/ma12142232

completely dissolved in the material but form separate phases or segregate to grain boundaries and surfaces. Segregation requires mobile dopants. Both oxygen and dopant (Sn) diffusion in ITO have been demonstrated to occur already at 300 °C [16–19].

If samples are processed at temperatures low enough to suppress oxygen diffusion and dopant segregation, defect equilibrium cannot be established. In such a case, the concentration of compensating defects could be lower than in equilibrium. Low processing temperatures of TCOs do therefore offer the potential advantage of achieving higher carrier concentrations. In contrast, in the case of In_2O_3, conductivities of films deposited at lower temperature ($\lesssim$ 200 °C) are in most cases lower than those of films prepared or annealed at higher temperature. In particular, films prepared at room temperature have conductivities below 10^3 S/cm, mostly because of lower carrier concentrations [20–24]. Films prepared at room temperature are often amorphous. In this case, the carrier concentration does not depend on donor concentration but is rather determined by the oxygen stoichiometry [25,26]. Enhanced crystallization of room temperature deposited films has been achieved using Fe_2O_3 seed layers [27]. Thereby, the carrier concentration can be enhanced by about one order of magnitude due to donor activation but remain below 10^{21} cm^{-3}.

Recently, Koida and coworkers have demonstrated that high conductivities of differently doped In_2O_3 films can be obtained by annealing room temperature deposited films to $\sim$ 200 °C [28–30]. There, the addition of H_2O during deposition can induce substantial grain growth during annealing and result in very high carrier mobilities of up to $\sim$ 140 cm^2/Vs. However, while the low temperature processing provides an advantage regarding temperature sensitive substrates and the high mobility leads to an enhanced optical transparency in the infrared, the films still exhibit carrier concentrations lower than 10^{21} cm^{-3}. There is yet no evidence that carrier concentration above 2×10^{21} cm^{-3} can be achieved by lower substrate temperatures.

As the conductivity of ITO is determined by a number of factors including crystallinity, grain size and oxygen content, which differently impact carrier concentration and mobility, it is difficult to discriminate between the different influences. This becomes particularly important for the identification of the conditions needed to achieve higher carrier concentrations by low temperature processing.

In the present work, we have studied the effect of low temperature ($\leq$ 200 °C) processing on the electrical properties of ITO thin films with different film thickness. Together with in-operando Hall effect measurements, it becomes possible to discriminate between the effects of crystallization, grain growth, donor activation and oxygen diffusion on carrier concentrations and mobilities. The results provide guidelines for low-temperature processing of doped In_2O_3 films and will be used to explain the effects of Al_2O_3 deposition on the electrical properties of ITO and the conditions for realizing defect modulation doping of this compound. Defect modulation doping utilizes a Fermi level in a contact phase, which is pinned by defects at a high energy [31]. Carrier concentrations higher than those observed by conventional doping can be achieved by this technique near an interface. A suitable material with a high Fermi energy is obtained by low-pressure atomic-layer-deposited Al_2O_3 [32].

2. Experimental

ITO and Al_2O_3 films were prepared in the Darmstadt Integrated SYstem for MATerials research (DAISY-MAT), which combines several home-made deposition chambers with a multi-technique surface analysis system in a single ultrahigh vacuum cluster tool [6]. ITO films were deposited on quartz glass substrates by magnetron sputtering with radio-frequency (RF) excitation. The background pressure of the deposition chamber was 10^{-6} Pa. A ceramic 2 inch ITO target with 10 wt% SnO_2 doping, a RF power of 25 W, a process pressure of 0.5 Pa, an Ar flux of 6.6 sccm and a target-to-substrate distance of 10 cm were used for deposition. The film thickness of ITO was varied from 8–200 nm and the substrate temperature during deposition from room temperature to 400°C.

Al_2O_3 was deposited using a low-pressure process in a separate vacuum chamber with a background pressure of 10^{-6} Pa using Trimethylaluminium (TMA) from SAFC Hitech and purified

Peer-reviewed version available at Materials 2019, 12, 2232; doi:10.3390/ma12142232

water as precursors. The setup and Al_2O_3 deposition are described in detail in [32]. The ALD pulse lengths were set using ALD 3 series valves (Swagelock) with a microelectronic control unit to 80 ms for TMA and 150 ms for water. Pumping continued during exposure and each exposure was followed by pumping for 300 s, resulting in a total duration of an ALD cycle of 10 min. The growth of aluminum oxide was carried out at a substrate temperature of 200 °C.

X-ray photoelectron spectroscopy (XPS) measurements were performed without breaking the vacuum using a Physical Electronics PHI 5700 (Physical Electronics Inc., Chanhassen, MN) spectrometer. Monochromatic Al Kα radiation at an emission angle of 45 ° and with an excitation energy of 1486.6 eV was used for XPS measurement. The binding energies of the spectrometer are regularly calibrated by a clean sputter cleaned silver sample. Coplanar grazing incidence X-ray diffraction (GIXRD) patterns were collected with a Bruker D8 Advance Series II (Bruker AXS, Karlsruhe, Germany) and a Rigaku SmartLab (Rigaku, Tokyo, Japan) diffractometer in the 2θ range of 15–85° using Cu Kα radiation with a weighted wavelength of 1.54186 Å. Room temperature and temperature dependent Hall-effect measurements were carried out in van-der-Pauw geometry using a custom-made setup, which allows for continuous measurements with controlled temperature, pressure and gas composition [18,33].

3. Results and Discussion

3.1. Influence of substrate temperature and film thickness

As a first step, the influence of substrate temperature on the electrical properties of ITO thin films with different thickness is presented in this section. Films deposited at elevated substrate temperature are expected to be crystalline but films grown at room temperature might be amorphous [20,25,34,35]. To verify this, X-ray diffraction patterns recorded in grazing incidence of the films deposited at room temperature are shown Fig. 1.

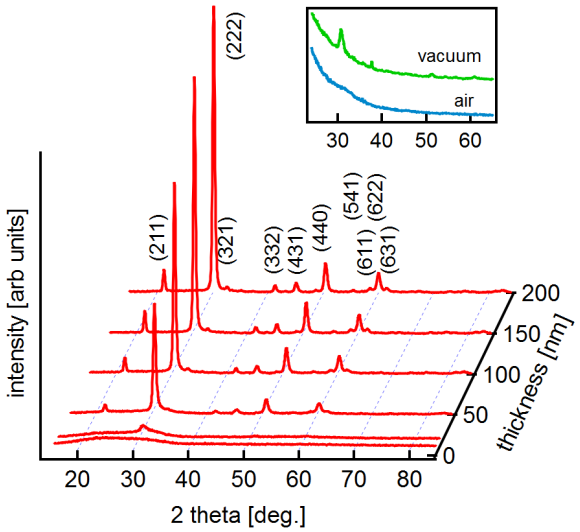

Figure 1. Grazing Incidence XRD patterns of ITO films with different film thickness deposited at room temperature. The indexed lattice planes correspond to those of cubic In_2O_3 (International Centre for Diffraction Data (ICDD) card 00-006-0416-High-bcc). The insert shows grazing incidence diffraction patterns of two 10 nm thick films annealed at 200 °C in air or vacuum, respectively (see section 3.2).

The thinnest film doesn't show any reflections. This is not due to the low film thickness as clear reflections are observed after annealing the same film (see insert; the effect of annealing is described in section 3.2). With increasing film thickness the diffraction peaks associated to In_2O_3 are

Peer-reviewed version available at Materials 2019, 12, 2232; doi:10.3390/ma12142232

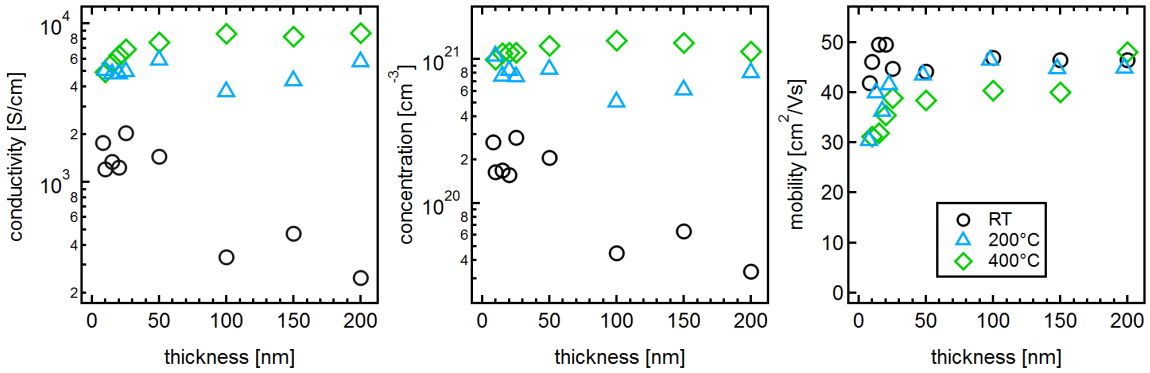

Figure 2. Conductivity (a), carrier concentration (b) and carrier mobility (c) of ITO films deposited at room temperature, 200 °C and 400 °C as a function of film thickness.

increasing. Hence, only the thinnest film is completely amorphous after deposition. The increasing crystallinity with film thickness has been observed previously and can be attributed, on one hand, to the energy of the impinging particles [36] and, on the other hand, to an increasing substrate temperature induced by the heat of condensation of the film [20,35]. Nevertheless, despite the observation of crystalline structure, it is expected that the crystallite size of the films grown at room temperature is substantially smaller than that of films grown at higher temperature. The films may also still contain some amorphous regions. The microstructure is important for understanding the dependence of electrical properties on film thickness and during annealing discussed below.

The conductivities, carrier concentrations and mobilities of films with thickness ranging from $10 - 200$ nm deposited at room temperature, 200 °C and 400 °C, respectively, are shown in Fig. 2. It is apparent that the conductivity of the films generally increases with deposition temperature, whereby Hall effect measurements demonstrate that this is mostly due to an increase of carrier concentration. The dependence of concentrations can at least partially be attributed to different concentrations of oxygen interstitials. It is reasonable that less oxygen is incorporated in the films at higher deposition temperature, due to a lower residence time of oxygen on the growing film's surface.

The carrier mobilities, which are shown at the right in Fig. 2, are rather independent on film thickness and substrate temperature with values $\sim 40\,\mathrm{cm}^2/\mathrm{Vs}$. This is not surprising for the films deposited at 200 °C and 400 °C, which have carrier concentrations near $10^{21}\,\mathrm{cm}^{-3}$. At such high carrier concentrations, grain boundary scattering, which is reducing the mobility at lower carrier concentrations below $\sim 10^{20}\,\mathrm{cm}^{-3}$ [19,37–39], is screened by the electron gas and the electron mobility is given by ionized impurity scattering, resulting in a carrier mobility of $\sim 40\,\mathrm{cm}^2/\mathrm{Vs}$ [40].

For the films deposited at room temperature, the situation is more complex, however. The carrier mobility of the thinnest films, which are amorphous, correspond well with those of amorphous ITO films reported in literature [26,27,34]. With increasing film thickness, however, the carrier concentration is reduced to values as low as $\sim 4 \times 10^{19}\,\mathrm{cm}^{-3}$. Given the polycrystalline nature of the thicker films deposited at room temperature, a lower carrier mobility is expected due to grain boundary scattering. It contrast, the mobility remains as high as that of films with higher carrier concentration. The unexpected high mobility of crystalline films with carrier concentrations $< 10^{20}\,\mathrm{cm}^{-3}$ deposited at room temperature are suggested to be related to the smaller grain size of the room temperature films. If the grains are very small, the depletion regions induced by the potential barriers at adjacent grain boundaries overlap, the bending of the energy bands will be reduced. The potential barrier for grain boundary scattering is then reduced according to the Seto model, which assumes the potential barrier to correspond to the band bending [37,38].

The conductivities of films deposited at different substrate temperature exhibit a different dependence on film thickness. For films deposited at 400°C the conductivity increases with film thickness. This can be explained by a thickness dependent change in grain size, which is common in

Peer-reviewed version available at Materials 2019, 12, 2232; doi:10.3390/ma12142232

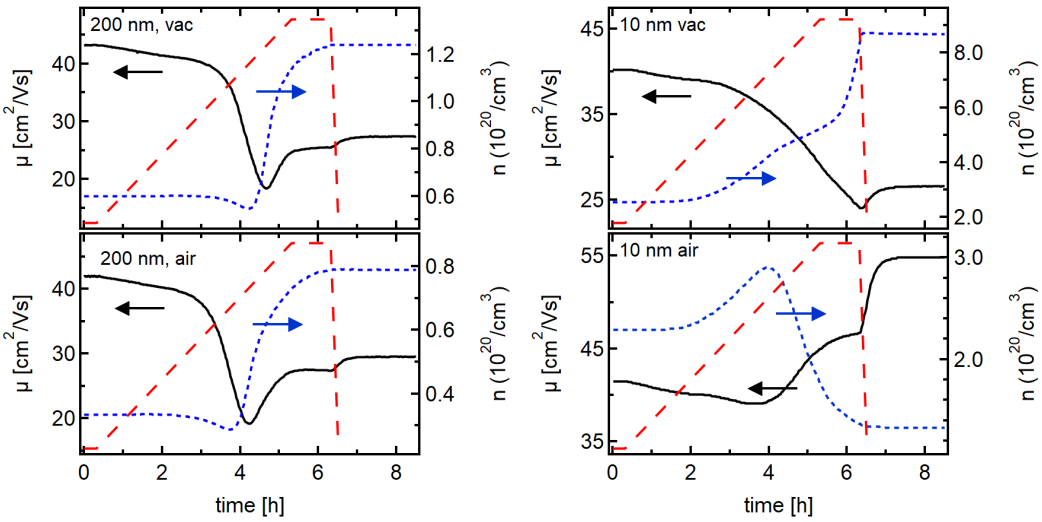

Figure 3. Hall effect measurements during annealing of 10 and 200 nm thick ITO films deposited at room temperature in vacuum or in air. The red dashed lines show the programmed temperature with a controlled heating ramp from 25°C–200°C and a holding time of 1 hour at 200°C.

film growth. In the presence of potential barriers at grain boundaries, which are the origin of grain boundary scattering, the average carrier concentration decreases when the grains become very small as in the initial stage of growth. An opposite behaviour with a conductivity decreasing with film thickness would be observed if the grain boundaries are more conductive than the grains as in the case of p-type Cu_2O [41].

The films deposited at room temperature exhibit a decrease of conductivity with increasing film thickness. This is due to the carrier concentration, which decreases by about one order of magnitude from 10 nm to 200 nm. On the one hand, the carrier concentration in the thinner, amorphous, films is determined by the coordination of the cations with oxygen, while the Sn-dopants remain ineffective [25,26]. One might therefore expect that the carrier concentration increases once the films crystallize with increasing film thickness and thereby activate the Sn donors. However, for a very small grain size of the thicker (crystalline) films grown at room temperature, the depletion regions of adjacent grain boundaries overlap. This does not only decrease the band bending, which affects the carrier mobility, but also decreases the average carrier concentration. While this is suggested to be the main reason for the lower carrier concentration of the thicker, crystalline, films deposited at room temperature, a higher oxygen incorporation may also contribute to this observation.

3.2. The effect of annealing

In the previous section it has been suggested that the low electrical conductivity of films deposited at room temperature is mostly determined by their microstructure, which is characterized by a very small grain size. In order to confirm this hypothesis, in-operando Hall effect measurements have been conducted during annealing of films deposited at room temperature. In order to follow the changes in conductivity, carrier concentration and mobility, samples were heated in vacuum (10^{-5} Pa) or in air with a rate of 0.5 K/min up to 200 °C and hold at that temperature for 1 hour. The results obtained for ITO films of 10 and 200 nm thickness are shown in Fig. 3.

The changes during heat treatment in vacuum or in air are almost identical for the 200 nm thick films. Only the magnitude of the carrier concentration is slightly different for the two studied samples. For both samples, the carrier concentration increases by about a factor of 2 and the carrier mobilities decrease first by a factor of 2 before it increases again slightly. Both carrier concentration and mobility saturate after 1 hour at 200 °C.

Peer-reviewed version available at Materials 2019, 12, 2232; doi:10.3390/ma12142232

The comparable behaviour upon annealing in vacuum and air indicates that the changes in carrier concentration are not related to a change in oxygen content, as that should depend on the annealing atmosphere. The fact that the oxygen content of the 200 nm films is not changing upon annealing is consistent with DFT calculations of oxygen diffusion [17] and with in-operando Hall effect measurements of crystalline ITO films [18], which indicate that oxygen diffusion at 200 °C is not fast enough.

Crystallization and grain growth can explain the increase in carrier concentration and the decrease of mobility upon heat treatment of the 200 nm thick films. Crystallization of amorphous regions, which might still be present in the 200 nm thick films deposited at room temperature, would activate the Sn donors [25,26] and thereby increase the carrier concentration. An increased carrier concentration will narrow the space charge regions at grain boundaries. The overlap between space charge regions of neighbouring space charge region will therefore be reduced and the band bending within the grain will be increased. This results in an increase of the average carrier concentration and an increase of the band bending between grain boundaries as illustrated in Fig. 4. The latter explains the decrease of carrier mobility. Grain growth will have a similar effect.

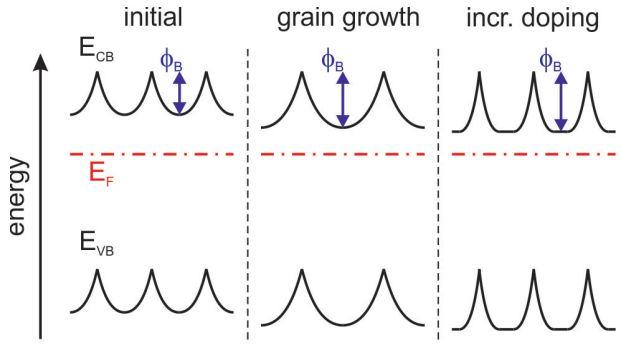

Figure 4. Energy band diagrams of n-type polycrystalline semiconductors with depleted electron concentrations in the space charge layers at grain boundaries. For very small grains, the potential profiles of neighbouring grain boundaries overlap. The band bending within the grain ϕ_B is increased upon grain growth or increase of doping concentration, which will result in an increase of average carrier concentration and in a reduction of carrier mobility.

In contrast to the 200 nm thick films, the annealing behaviour of the 10 nm thick films is drastically different for annealing in vacuum and air. Annealing in vacuum results in a behaviour which is similar to that of the 200 nm thick films. However, in contrast to the thicker films, the carrier concentration and the mobility do not saturate after 1 hour at 200 °C. In contrast, after an initial decrease during ramping up the temperature, the carrier concentration of the 10 nm thick decreases during annealing in air. The different carrier concentration after annealing in vacuum and air indicates that the effective doping concentration in the films increases during annealing in vacuum. This is consistent with the much higher increase of carrier concentration of the 10 nm vacuum annealed film compared to that of the 200 nm thick films. Not only the increase is much higher, also the starting level is much higher.

The annealing atmosphere has also an effect on the crystallization behaviour, which is illustrated in the insert of Fig. 1. Grazing incidence X-ray diffraction only shows lattice reflections after annealing in vacuum. The film annealed in air remains amorphous, for reasons which remain unclear. The different crystallinity is also reflected by the change of carrier mobility during cooling of the samples at the end of the annealing process (see Fig. 3). The air annealed, amorphous, film shows a much higher increase in mobility during cooling from 200°C to room temperature than the other three samples. An increase of μ with decreasing temperature is expected for ionized impurity scattering. A lower or even inverted temperature dependence indicates the presence of grain boundary scattering [19]. Grain boundary scattering should thus not contribute to the temperature dependence of the air annealed 10 nm film, which is consistent with the amorphous structure.

Peer-reviewed version available at Materials 2019, 12, 2232; doi:10.3390/ma12142232

The decrease of carrier concentration and increase of mobility during air annealing of the 10 nm thick film can both be explained by incorporation of oxygen. Medvedeva and coworkers have clearly demonstrated that the carrier concentration in amorphous doped In_2O_3 films is determined by the oxygen stoichiometry [26]. Addition of oxygen will therefore reduce the carrier concentration and, by the concomitant reducing of ionized impurities, also raise the mobility.

Two effects contribute to the increase of doping concentration during vacuum annealing of the 10 nm thick film: i) the activation of the Sn dopants due to crystallization and ii) the extraction or incorporation of oxygen. It has been argued above that the latter is not important for the 200 nm thick films. But, the time τ required to establish equilibrium by bulk diffusion (of oxygen) depends on the square of the film thickness L and is given by $\tau = L^2/\pi^2 D$, where D is the diffusion coefficient [42]. It is therefore not unlikely that oxygen diffusion can be important for very thin films but not for thicker ones at 200°C.

To further check whether the removal of oxygen contributes to the strong increase of carrier concentration of the 10 nm film during vacuum annealing, an extended annealing experiment has been carried out. The measurement is shown in Fig. 5.

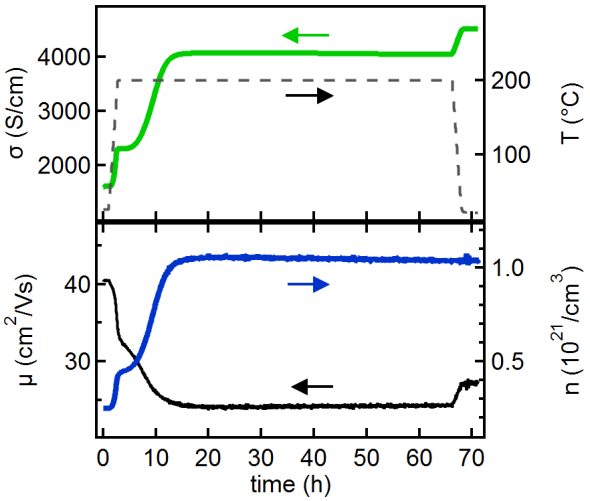

Figure 5. Conductivity and Hall effect measurements during extended annealing of a 10 nm thick ITO film deposited at room temperature in vacuum.

In contrast to the curve shown in Fig. 3, there is a clear saturation of carrier concentration and mobility after $\sim$ 15 hours annealing at 200 °C. The saturated carrier concentration amounts to $n \approx 1.05 \times 10^{21}$ cm^{-3}, which is higher than those observed for deposition at 200 °C (see Fig. 2). After cooling down to room temperature, a conductivity of 4520 S/cm is reached. This is of the same magnitude as those obtained with films of the same thickness at higher deposition temperatures. Vacuum annealing is therefore suitable to obtain highest conductivities with very thin films. The required annealing times are, however, rather long, as shown by the presented in-operando Hall effect study. The in-operando measurements demonstrate that annealing experiments with fixed (shorter) annealing times and post-anneal analysis can only provide a snapshot of the effects of annealing, which make an analysis of the origin of the changes of electrical properties very difficult.

The very high carrier concentrations reached after long vacuum annealing of the 10 nm film can only be reached if oxygen is extracted from the films during annealing. This can be concluded by comparison with ITO films grown under identical process conditions at room temperature but on Fe_2O_3 seed layers [27]. The Fe_2O_3 seed layers strongly enhance crystallization at room temperature, which results in a substantial increase of carrier concentration and conductivity due to donor activation and increased grain size. The carrier concentrations reached with Fe_2O_3 seed layers are, however, lower than 6.5×10^{20} cm^{-3}. Donor activation by crystallization is therefore not sufficient to explain the

Peer-reviewed version available at Materials 2019, 12, 2232; doi:10.3390/ma12142232

carrier concentration higher than 10^{21} cm^{-3} reached by vacuum annealing. The effect of annealing in dependence on film thickness and atmosphere are summarized in Fig. 6.

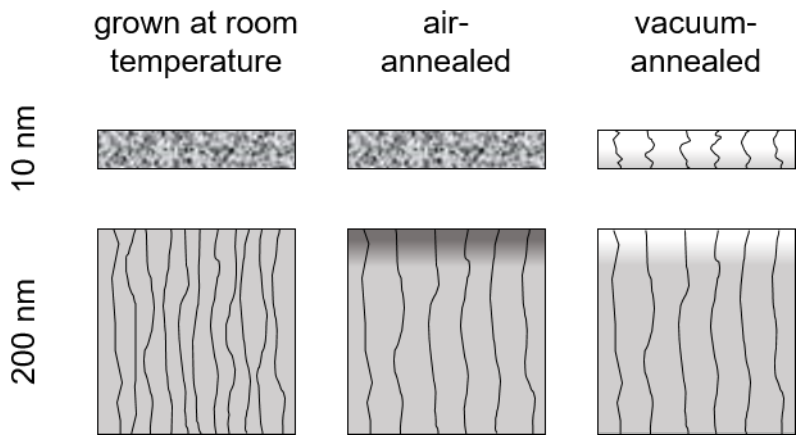

Figure 6. Effect of annealing of 10 and 200 nm thick ITO films deposited at room temperature. The annealing was performed with a heating rate of 0.5 K/min up to 200 °C and a holding time of 1 h either in vacuum or in air. Curved lines indicate grain boundaries and fill colour the oxygen concentration. The filling style of the as-grown 10 nm thick sample indicates an amorphous structure.

3.3. Effect of Al_2O_3 deposition

X-ray photoelectron spectra of 20 and 200 nm thick ITO films deposited at room temperature before and after 5 ALD cycles of Al_2O_3, corresponding to an Al_2O_3 thickness of 0.5 nm, are shown in Fig. 7. The binding energies of the uncoated 20 nm thick film are higher than those of the uncoated 200 nm thick film. This corresponds well with the higher carrier concentration of the thinner film discussed in section 3.1. The deposition of Al_2O_3 results in the appearance of Al 2p and Al 2s emissions (not shown) and a reduction of the intensities of the In 3d core level and the valence band emission. After Al_2O_3 deposition, the O 1s line exhibits a pronounced additional emission at a binding energy of $\sim$ 532 eV, which can be assigned to oxygen in the Al_2O_3 layer. In agreement to previous work [32], where Al_2O_3 films were grown by ALD onto ITO films deposited at 400°C, the binding energies of the ITO substrate are increased by the Al_2O_3 deposition. This corresponds to a rise of the Fermi energy and indicates the formation of a surface electron accumulation layer. Such layers have been frequently reported to be present at In_2O_3 surfaces [43–46]. We like to point out that no accumulation layer is present on the as-deposited surfaces, as the samples have not been exposed to air before XPS measurement [6].

The upward shift of the Fermi energy after Al_2O_3 deposition can partially be assigned to a reduction of the substrate, which is indicated for the 20 nm thick film in Fig. 7 by the appearance of a shoulder on the low binding energy side of the In 3d emission (indicated by an asterisk in Fig. 7) and by the increased band gap emission in the valence band spectrum. However, the Fermi energy in the Al_2O_3 films deposited by the low-pressure process in our system is reproducibly pinned at 4.5 eV above the valence band maximum, independent on substrate [31,32,47,48]. Together with a very small valence band offset between ITO and Al_2O_3 in the absence of pinning [32], it is expected that the Fermi energy in the ITO also raises to $E_F - E_{VB} > 4$ eV. The binding energies of the ITO substrate do not correspond to such high Fermi energies but only to $E_F - E_{VB} \approx 3.3$ eV. This is likely explained by the formation of a very narrow space charge region at the surface of the highly doped ITO, which is narrower than the depth probed by XPS. The situation corresponds to an effective modification of the band alignment [32].

Conductivity and Hall effect measurements performed on ITO films deposited at room temperature are shown in Fig. 8 together with those obtained after Al_2O_3 deposition. Data for

Peer-reviewed version available at Materials 2019, 12, 2232; doi:10.3390/ma12142232

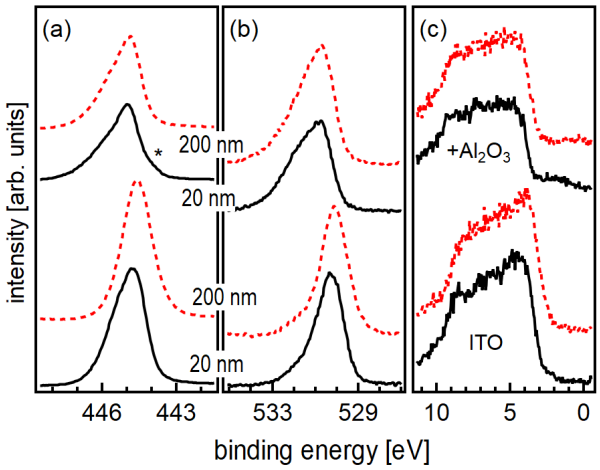

Figure 7. In3d (a), O1s (b) and valence band (c) X-ray photoelectron spectra of 20 nm (solid black lines) and 200 nm (dashed red lines) thick ITO films before (bottom) and after (top) deposition of Al_2O_3 using 5 ALD cycles. The asterisk indicates a shoulder in the In 3d spectrum, which corresponds to a partial reduction of In.

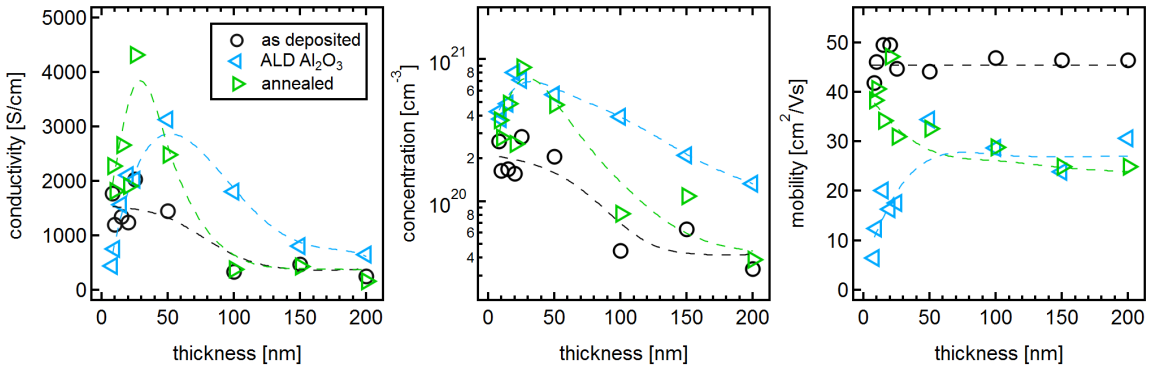

Figure 8. Hall effect measurements as a function of film thickness of ITO films deposited at room temperature (black circles), ITO films deposited at room temperature after Al_2O_3 deposition, and ITO films deposited at room temperature after annealing in the ALD chamber (ALD-anneal) in vacuum at 200°C. The data of the as-deposited films are the same as those in Fig. 2. Dashed lines are a guide to the eye.

uncoated samples are the same as those shown in Fig. 2. After Al_2O_3 deposition, the conductivity of the films is lower/higher than without Al_2O_3 for films thinner/thicker than $\sim$ 15 nm. This behaviour is contradictory to defect modulation doping, which has been shown to increase the conductivity for 10 nm thick SnO_2 films [31]. As modulation doping should affect only the near interface region, no substantial change of electrical properties has to be expected for thicker films.

The carrier concentration is increased by Al_2O_3 deposition, independent on film thickness in accordance with the raise of the Fermi level. The highest carrier concentrations of $n \approx 8 \times 10^{20}$ cm^{-3} are obtained for 20 and 25 nm thick films. It is the increase of carrier concentration, which explains the increase of conductivity by Al_2O_3 deposition for films thicker than 15 nm. For films thinner than 15 nm, the reduction of conductivity by Al_2O_3 deposition is caused by a significant lowering of the mobility.

The Al_2O_3 deposition is performed in vacuum chamber at 200 °C and involves heating of the samples in vacuum before exposure to the process gas. As indicated by the results described in section 3.2, the heating process in vacuum strongly affects the electrical properties. To discriminate between the effects of annealing and Al_2O_3 deposition, additional samples were annealed in the ALD chamber under the conditions present during the ALD process, just without exposure to TMA and H_2O. This

Peer-reviewed version available at Materials 2019, 12, 2232; doi:10.3390/ma12142232

annealing, which is referred to as ALD-anneal here, is shorter than the one performed in the Hall effect setup. Conductivity and Hall effect measurements performed after the ALD-anneal are also shown in the Fig. 8.

The dependence of carrier concentration on film thickness after the ALD anneal is comparable to the behaviour described in section 3.2. Except for the 200 nm thick film, the carrier concentrations of thicker films are 10^{20} cm^{-3}. For thinner films values of up to 8×10^{20} cm^{-3} are reached. This behaviour has been explained in section 3.2 by grain growth and, for the thinner films, by donor activation and oxygen extraction. Up to an ITO thickness of 50 nm, the carrier concentrations of the ALD-annealed samples and of those coated with Al_2O_3 are the same within the experimental uncertainty. This again rules out the presence of modulation doping. For films thicker than 50 nm, the Al_2O_3-coated films exhibit higher carrier concentrations than the ALD-annealed ones. Apparently, the exposure to Al_2O_3 is more reducing than vacuum alone, in agreement with the partial reduction of the films observed by XPS.

Al_2O_3 deposition results in a strong reduction of mobility for samples with thickness < 50 nm. This reduction is not related to the high temperature but must be caused by the ALD process. It is probably related to the chemical reduction of the film, which is indicated by XPS in Fig. 7. The strong reduction of the film might increase grain boundary potential barriers, which have been related to reduced Sn (Sn^{+II}) at the grain boundaries [19]. Extraction of oxygen from grain boundaries would then increase the density of trapping centers and increase the potential barrier height. As the effect will be restricted to the surface region due to the limited diffusivity of oxygen at 200 °C, the observed increase of mobility of the Al_2O_3 coated films with ITO thickness is reasonable.

The absence of a modulation doping effect upon Al_2O_3 deposition, which has been clearly demonstrated for SnO_2 [31] and which may also contribute to the formation of two-dimensional electron gases at $SrTiO_3$ interfaces with Al_2O_3 [49,50], is very likely related to the high mobility of defect species. The annealing experiments discussed in section 3.2 clearly demonstrate that oxygen defects are sufficiently mobile to diffuse several nanometers during processing at the Al_2O_3 deposition temperature of 200 °C. The compensating oxygen interstitial defects will then diffuse towards the interface to screen the potential difference induced by the high Fermi energy at the interface [51]. The condition required to enable defect modulation doping, which is the kinetic suppression of equilibrium concentrations, is not met with ITO at 200 °C. Lower processing temperatures for ALD deposition, which has been demonstrated in literature [52,53], would be required.

4. Summary and Conclusions

Low-temperature processed ITO thin films offer the potential of overcoming the doping limit by suppressing the equilibrium of compensating oxygen interstitial defects. The aim of this work was to provide a more detailed understanding of the processes, which determine the carrier concentrations of ITO films processed at substrate temperature where oxygen diffusion and cation segregation is suppressed. For this purpose, electrical properties of Sn-doped In_2O_3 (ITO) thin films as a function of film thickness have been presented and discussed. Films deposited at room temperature exhibit significantly lower conductivities compared to films deposited at 200 and 400 °C. The differences are caused by different carrier concentrations, while the mobilities are rather insensitive on deposition temperature and film thickness.

Only the thinnest films deposited in our setup at room temperature are amorphous. The intensity of diffraction peaks increases with increasing film thickness, which has been assigned to a slow increase of substrate temperature with deposition time and to ion bombardment effects. The carrier concentration of the room temperature deposited films decreases with film thickness. As the carrier mobility is not affected by the reduced carrier concentration, which would be expected for grain boundary scattering, the reduction of n is explained by the formation of very small grains with overlapping space charge regions.

Peer-reviewed version available at *Materials* **2019**, *12*, 2232; doi:10.3390/ma12142232

Room temperature deposited 10 nm thick amorphous and 200 nm thick crystalline films have been annealed in vacuum and air at 200 °C. Conductivity and Hall effect measurements were recorded during the complete annealing cycles. The thicker films exhibit a slight increase in carrier concentration and reduction of mobility during annealing, regardless of the annealing atmosphere. The changes can be explained by grain growth. A change of effective doping concentration by variation of the oxygen content can be excluded. This is consistent with previous experiments and calculations on oxygen diffusivity. A change of oxygen content is, however, evident for the 10 nm thick films. Annealing in vacuum results in a substantial increase of carrier concentration by almost an order of magnitude to $n > 10^{21}$ cm^{-3}, while annealing in air results in a decrease of carrier concentration. It is noted that annealing in air does, in contrast to annealing in vacuum, not lead to crystallization of the 10 nm thick films.

During annealing at 200 °C, diffusion of oxygen does therefore only affect a very thin region near the surface of thicker films. Manipulating the carrier concentrations in thicker films is therefore not an option at this temperature. The remaining diffusivity of compensating oxygen defects at 200 °C is, however, sufficient to screen the high Fermi level induced by deposition of Al_2O_3 using atomic layer deposition. This disables the use of defect modulation doping at this temperature. But, the growth of Al_2O_3 at lower substrate temperatures remains an option.

Apart from the fact that defect modulation doping at lower temperatures cannot be ruled out at present, it does not seem possible to achieve carrier concentrations approaching those observed with the electrochemical reduction technique by post-deposition treatments. A realization of such carrier concentrations using a suitable deposition at low-substrate temperature appears more realistic. With such a process, the inherently small grain size of low-temperature grown films has to be overcome, as this clearly limits carrier concentrations. The use of seed layers, such as the recently demonstrated Fe_2O_3 might be a solution for this [27].

Author Contributions: Thin film deposition, electrical and XPS analysis was performed by G K D, X-ray diffraction by H R and J B and additional conductivity measurements by J H. Discussion and interpretation of results was conducted by G K D, D B and A K. The Manuscript was written by and G K D and A K and revised by all authors; Funding has been acquired by D B and A K.

Funding: This work was carried out in the framework of EJD-FunMat (European Joint Doctorate for Multifunctional Materials) and has received funding from the European Union's Horizon 2020 research and innovation programme under the Marie Sklodowska-Curie grant agreement No 641640.

Acknowledgments: The authors acknowledge the Consortium des Moyens Technologiques Communs (CMTC) - Grenoble INP platform for diffraction characterization equipment.

Conflicts of Interest: The authors declare no conflict of interest. The founding sponsors had no role in the design of the study; in the collection, analyses, or interpretation of data; in the writing of the manuscript, and in the decision to publish the results.

Abbreviations

The following abbreviations are used in this manuscript:

ALD	atomic-layer-deposition
ITO	Sn-doped In_2O_3
XPS	X-ray photoelectron spectroscopy
XRD	X-ray diffraction

References

1. Ginley, D.S.; Hosono, H.; Paine, D.C., Eds. *Handbook of Transparent Conductors*; Springer: New York, 2010.
2. Ellmer, K. Past achievements and future challenges in the development of optically transparent electrodes. *Nature Photonics* **2012**, *6*, 809–817.
3. Battaglia, C.; Cuevas, A.; Wolf, S.D. High-efficiency crystalline silicon solar cells: status and perspectives. *Energy Environ. Sci.* **2016**, *9*, 1552–1576.

Peer-reviewed version available at Materials 2019, 12, 2232; doi:10.3390/ma12142232

4. So, F.; Kido, J.; Burrows, P. Organic Light-Emitting Devices for Solid-State Lighting. *MRS Bull.* **2008**, *33*, 663–669.
5. Riedl, T.; Gorrn, P.; Kowalsky, W. Transparent Electronics for See-Through AMOLED Displays. *J. Display Technol.* **2009**, *5*, 501–508.
6. Klein, A. Transparent Conducting Oxides: Electronic Structure – Property Relationship from Photoelectron Spectroscopy with in-situ Sample Preparation. *J. Am. Ceram. Soc.* **2013**, *96*, 331–345.
7. Tahar, R.B.H.; Ban, T.; Ohya, Y.; Takahashi, Y. Tin doped indium oxide thin films: Electrical properties. *J. Appl. Phys.* **1998**, *83*, 2631–2645.
8. Walukiewicz, W. Intrinsic limitations to the doping of wide-gap semiconductors. *Physica B* **2001**, *302-303*, 123–134.
9. Robertson, J.; Clark, S.J. Limits to doping in oxides. *Phys. Rev. B* **2011**, *83*, 075205.
10. Lany, S.; Zunger, A. Dopability, Intrinsic Conductivity, and Nonstoichiometry of Transparent Conducting Oxides. *Phys. Rev. Lett.* **2007**, *98*, 045501.
11. Frank, G.; Köstlin, H. Electrical Properties and Defect Model of Tin-Doped Indium Oxide Layers. *Appl. Phys. A* **1982**, *27*, 197–206.
12. González, G.B.; Mason, T.O.; Quintana, J.P.; Warschkow, O.; Ellis, D.E.; Hwang, J.H.; Hodges, J.P. Defect structure studies of bulk and nano-indium-tin oxide. *J. Appl. Phys.* **2004**, *96*, 3912–3920.
13. Yamada, N.; Yasui, I.; Shigesato, Y.; Li, H.; Ujihira, Y.; Nomura, K. Doping Mechanisms of Sn in In_2O_3 Powder Studied Using ^{119}Sn Mössbauer Spectroscopy and X-Ray Diffraction. *Jpn. J. Appl. Phys.* **1999**, *38*, 2856–2862.
14. Ágoston, P.; Erhart, P.; Klein, A.; Albe, K. Geometry, electronic structure and thermodynamic stability of intrinsic point defects in indium oxide. *J. Phys.: Condens. Matter* **2009**, *21*, 455801.
15. Ágoston, P.; Körber, C.; Klein, A.; Puska, M.J.; Nieminen, R.M.; Albe, K. Limits for n-type doping in In_2O_3 and SnO_2: A theoretical approach by first-principles calculations using hybrid-functional methodology. *J. Appl. Phys.* **2010**, *108*, 053511.
16. Gassenbauer, Y.; Schafranek, R.; Klein, A.; Zafeiratos, S.; Hävecker, M.; Knop-Gericke, A.; Schlögl, R. Surface states, surface potentials and segregation at surfaces of tin-doped In_2O_3. *Phys. Rev. B* **2006**, *73*, 245312.
17. Ágoston, P.; Albe, K. Ab initio modeling of diffusion in indium oxide. *Phys. Rev. B* **2010**, *81*, 195205.
18. Hohmann, M.V.; Wachau, A.; Klein, A. In situ Hall effect and conductivity measurements of ITO thin films. *Solid State Ionics* **2014**, *262*, 636–639.
19. Frischbier, M.V.; Wardenga, H.F.; Weidner, M.; Bierwagen, O.; Jia, J.; Shigesato, Y.; Klein, A. Influence of dopant species and concentration on grain boundary scattering in degenerately doped In_2O_3 thin films. *Thin Solid Films* **2016**, *614*, 62–68.
20. Song, P.K.; Akao, H.; Kamei, M.; Shigesato, Y.; Yasui, I. Preparation and Crystallization of Tin-doped and Undoped Amorphous Indium Oxide Films Deposited by Sputtering. *Jpn. J. Appl. Phys.* **1999**, *38*, 5224.
21. Nunes de Carvalho, C.; Luis, A.; Lavareda, G.; Fortunato, E.; Amaral, A. Effect of thickness on the properties of ITO thin films deposited by RF-PERTE on unheated, flexible, transparent substrates. *Surface and Coatings Technology* **2002**, *151-152*, 252–256.
22. Kim, D.; Han, Y.; Cho, J.S.; Koh, S.K. Low temperature deposition of ITO thin films by ion beam sputtering. *Thin Solid Films* **2000**, *377-378*, 81–86.
23. Hao, L.; Diao, X.; Xu, H.; Gu, B.; Wang, T. Thickness dependence of structural, electrical and optical properties of indium tin oxide (ITO) films deposited on PET substrates. *Appl. Surf. Sci.* **2008**, *254*, 3504–3508.
24. Kim, S.T.; Kim, T.G.; Cho, H.; Yoon, S.J.; Kim, H.S.; Kim, J.K. Thickness Dependence of Properties of ITO Films Deposited on PET Substrates. *J. Nanosci. Nanotechnol.* **2016**, *16*, 1852–1854.
25. Bellingham, J.R.; Phillips, W.A.; Adkins, C.J. Electrical and optical properties of amorphous indium oxide. *J. Phys.: Condens. Matter* **1990**, *2*, 6207–6221.
26. Medvedeva, J.E.; Buchholz, D.B.; Chang, R.P.H. Recent advances in understanding the structure and properties of amorphous oxide semiconductors. *Adv. Electr. Mater.* **2017**, *3*, 1700082.
27. Lohaus, C.; Steinert, C.; Deyu, G.; Brötz, J.; Jaegermann, W.; Klein, A. Enhancing electrical conductivity of room temperature deposited Sn-doped In_2O_3 thin films by hematite seed layers . *Appl. Phys. Lett.* **2018**, *112*, 152105.

Peer-reviewed version available at Materials 2019, 12, 2232; doi:10.3390/ma12142232

28. Koida, T.; Ueno, Y.; Shibata, H. In_2O_3-Based Transparent Conducting Oxide Films with High Electron Mobility Fabricated at Low Process Temperatures. *phys. stat. sol. (a)* **2018**, *215*, 1700506.
29. Koida, T.; Fujiwara, H.; Kondo, M. Hydrogen-doped $In_2O_3$3 as high-mobility transparent conductive oxide. *Jpn. J. Appl. Phys.* **2007**, *46*, L685–L687.
30. Koida, T.; Kondo, M.; Tsutsumi, K.; Sakaguchi, A.; Suzuki, M.; Fujiwara, H. Hydrogen-doped In_2O_3 transparent conducting oxide films prepared by solid-phase crystallization method. *J. Appl. Phys.* **2010**, *107*.
31. Weidner, M.; Fuchs, A.; Bayer, T.J.M.; Rachut, K.; Schnell, P.; Deyu, G.K.; Klein, A. Defect Modulation Doping. *Adv. Funct. Mater.* **2019**, *29*, 1807906.
32. Bayer, T.J.M.; Wachau, A.; Fuchs, A.; Deuermeier, J.; Klein, A. Atomic layer deposition of Al_2O_3 onto Sn-doped In_2O_3: Absence of self-limited adsorption during initial growth by oxygen diffusion from the substrate and band offset modification by Fermi level pinning in Al_2O_3. *Chem. Mater.* **2012**, *24*, 4503–4510.
33. Wardenga, H.; Frischbier, M.V.; Morales-Masis, M.; Klein, A. In-situ Hall-effect monitoring of vacuum annealing of In_2O_3:H thin films. *Materials* **2015**, *8*, 561–574.
34. Khanal, R.; Buchholz, D.B.; Chang, R.P.H.; Medvedeva, J.E. Composition-dependent structural and transport properties of amorphous transparent conducting oxides. *Phys. Rev. B* **2015**, *91*, 205203.
35. Park, J.O.; Lee, J.H.; Kim, J.J.; Cho, S.H.; Cho, Y.K. Crystallization of indium tin oxide thin films prepared by RF-magnetron sputtering without external heating. *Thin Solid Films* **2005**, *474*, 127–132.
36. Mattox, D.M. Particle bombardment effects on thin-film deposition: A review. *J. Vac. Sci. Technol. A* **1989**, *7*, 1105–1114.
37. Seto, J.Y.W. The electrical properties of polycrystalline silicon films. *J. Appl. Phys.* **1975**, *46*, 5247–5254.
38. Ellmer, K. Electrical Properties. In *Transparent Conductive Zinc Oxide*; Ellmer, K.; Klein, A.; Rech, B., Eds.; Springer: Berlin, 2008; pp. 35–78.
39. Sommer, N.; Hüpkes, J.; Rau, U. Field Emission at Grain Boundaries: Modeling the Conductivity in Highly Doped Polycrystalline Semiconductors. *Phys. Rev. Appl.* **2016**, *5*, 024009.
40. Preissler, N.; Bierwagen, O.; Ramu, A.T.; Speck, J.S. Electrical transport, electrothermal transport, and effective electron mass in single-crystalline In_2O_3 films. *Phys. Rev. B* **2013**, *88*, 085305.
41. Deuermeier, J.; Wardenga, H.F.; Morasch, J.; Siol, S.; Nandy, S.; Calmeiro, T.; Martins, R.; Klein, A.; Fortunato, E. Highly conductive grain boundaries in copper oxide thin films. *J. Appl. Phys.* **2016**, *119*, 235303.
42. Crank, J. *The Mathematics of Diffusion*; Oxford University Press: Oxford, 1975.
43. King, P.D.C.; Veal, T.D.; Payne, D.J.; Bourlange, A.; Egdell, R.G.; McConville, C.F. Surface Electron Accumulation and the Charge Neutrality Level in In_2O_3. *Phys. Rev. Lett.* **2008**, *101*, 116808.
44. King, P.D.C.; Veal, T.D.; Fuchs, F.; Wang, C.Y.; Payne, D.J.; Bourlange, A.; Zhang, H.; Bell, G.R.; Cimalla, V.; Ambacher, O.; Egdell, R.G.; Bechstedt, F.; McConville, C.F. Band gap, electronic structure, and surface electron accumulation of cubic and rhombohedral In_2O_3. *Phys. Rev. B* **2009**, *79*, 205211.
45. Bierwagen, O. Indium oxide—a transparent, wide-band gap semiconductor for (opto)electronic applications. *Semicond. Sci. Technol.* **2015**, *30*, 024001.
46. Berthold, T.; Rombach, J.; Stauden, T.; Polyakov, V.; Cimalla, V.; Krischok, S.; Bierwagen, O.; Himmerlich, M. Consequences of plasma oxidation and vacuum annealing on the chemical properties and electron accumulation of In_2O_3 surfaces. *J. Appl. Phys.* **2016**, *120*, 245301.
47. Hillmann, S.; Rachut, K.; Bayer, T.J.M.; Li, S.; Klein, A. Application of atomic layer deposited Al_2O_3 as charge injection layer for high-permittivity dielectrics . *Semicond. Sci. Technol.* **2015**, *30*, 024012.
48. Deuermeier, J.; Bayer, T.; Yanagi, H.; Kiazadeh, A.; Martins, R.; Klein, A.; Fortunato, E. Substrate reactivity as origin of Fermi level pinning at the Cu_2O/ALD-Al_2O_3 interface. *Mater. Res. Expr.* **2016**, *3*, 046404.
49. Lee, S.W.; Liu, Y.; Heo, J.; Gordon, R.G. Creation and Control of Two-Dimensional Electron Gas Using Al-Based Amorphous Oxides/$SrTiO_3$ Heterostructures Grown by Atomic Layer Deposition. *Nano Letters* **2012**, *12*, 4775–4783.
50. Chen, Y.Z.; Bovet, N.; Trier, F.; Christensen, D.V.; Qu, F.M.; Andersen, N.H.; Kasama, T.; Zhang, W.; Giraud, R.; Dufouleur, J.; Jespersen, T.S.; Sun, J.R.; Smith, A.; Nygård, J.; Lu, L.; Büchner, B.; Shen, B.G.; Linderoth, S.; Pryds, N. A high-mobility two-dimensional electron gas at the spinel/perovskite interface of c-Al_2O_3/$SrTiO_3$. *Nature Commun.* **2013**, *4*, 1371.

Peer-reviewed version available at Materials 2019, 12, 2232; doi:10.3390/ma12142232

51. Gregori, G.; Merkle, R.; Maier, J. Ion conduction and redistribution at grain boundaries in oxide systems. *Prog. Mater. Sci.* **2017**, *89*, 252–305.
52. Groner, M.D.; Fabreguette, F.H.; Elam, J.W.; George, S.M. Low-Temperature Al_2O_3 Atomic Layer Deposition. *Chem. Mater.* **2004**, *16*, 639–645.
53. Kot, M.; Das, C.; Wang, Z.; Henkel, K.; Rouissi, Z.; Wojciechowski, K.; Snaith, H.J.; Schmeisser, D. Room-Temperature Atomic Layer Deposition of Al_2O_3: Impact on Efficiency, Stability and Surface Properties in Perovskite Solar Cells. *ChemSusChem* **2016**, *9*, 3401–3406.